Journal of Building Engineering 80 (2023) 108009

Contents lists available at ScienceDirect

Journal of Building Engineering

journal homepage: www.elsevier.com/locate/jobe

Experimental energy performance assessment of a bifacial photovoltaic system and effect of cool roof coating

Daniel Valencia-Caballero [a,*], Salim Bouchakour [b], Alvaro Luna [c], Borja Garcia-Marco [c], Ana Huidobro [a], Iván Flores-Abascal [d], Asier Sanz [a], Eduardo Román [a]

[a] TECNALIA, Basque Research and Technology Alliance (BRTA), Paseo Mikeletegi 2, San Sebastián, 20009, Spain
[b] Centre de Développement des Energies Renouvelables, CDER, Algiers, 16340, Algeria
[c] Department of Electrical Engineering Universitat Politècnica de Catalunya, 08222, Terrassa, Spain
[d] ENEDI Research Group, Energy Engineering Department, Faculty of Engineering of Bilbao, University of the Basque Country (UPV/EHU), Pza. Ingeniero Torres Quevedo 1, Bilbao, 48013, Spain

ARTICLE INFO

Keywords:
Bifacial PV
Cool roof
BAPV
Building energy performance
Photovoltaic

ABSTRACT

In the quest for high albedo materials that boost the energy production of bifacial photovoltaic systems, a range of material already exists for reducing building roof surface temperatures, called cool roof materials. However, there is a noticeable absence of scientific literature addressing the combination of cool roofs and bifacial photovoltaic systems. This study investigates the photovoltaic performance of a bifacial photovoltaic system with cool roof coating on the underside and its impact on floor temperature. For this purpose, four ~1kWp prototypes were installed on the terrace of the GAIA building of the UPC near Barcelona, Spain: (1) bifacial panels above a cool roof, (2) bifacial panels above normal floor, (3) bifacial panels above a normal floor with n-type solar cells encapsulated in TPO, and (4) monofacial panels. The results reveal 8.6 % higher PV yield for bifacial with cool roof compared to monofacial, and 4–4.5 % higher for bifacial (normal floor) compared to monofacial. Additionally, the cool roof coating contributes to reducing the floor temperatures, particularly in the unshaded (exposed) areas during summer (−3.8 °C). The presence of photovoltaic panels has also demonstrated a positive impact on floor temperatures during both winter and summer. Thus, the cool roof coating offers two benefits: increased photovoltaic yield and reduced building cooling requirements, both of which are associated with economic advantages. The cool roof coating can be integrated into existing or new bifacial roof systems.

Nomenclature

BAPV –	Building added/attached/applied photovoltaics
BIPV –	Building integrated photovoltaics
BR –	Bifacial Ratio
CR –	Cool Roof
G -	Incident solar radiation [W/m^2]

* Corresponding author.
E-mail address: daniel.valencia@tecnalia.com (D. Valencia-Caballero).

https://doi.org/10.1016/j.jobe.2023.108009
Received 14 July 2023; Received in revised form 19 October 2023; Accepted 23 October 2023
Available online 2 November 2023

GCR – Ground Coverage Ratio
GHI – Global Horizontal Irradiance
HR – High reflectance. In reference to Cool Roof coated floor
P_{DC} - PV electrical power produced in DC [W]
Period w/o sh – Period without shades, i.e. excluding from November to February
POA – Plane-of-Array
S - PV field active surface [m^2]
STC – Standard Test Conditions
η_{op} - Operational efficiency

1. Introduction

The energy intensity of buildings, representing the total final energy consumption per square metre, has remained unchanged over the last three years at around 150 kWh/m2. To achieve the needed pathway toward net zero carbon, the International Energy Agency estimates that intensity needs to drop by around 35% of its current level to around 95 kWh/m2 [1]. Thus, several policies are being taken to mitigate this issue. However, this can be achieved not only by reducing energy consumption but also by generating energy with renewable energy systems in buildings.

One of these solutions is the photovoltaic modules, which can be used in or on the building envelope, either integrated as building products (BIPV) [2,3] or applied (BAPV) [4] without any building function. The second group includes rooftop PV systems, that are usually installed on terraces or flat roofs. In this sense, the recent massive deployment of bifacial modules [5] has also been extended to these applications. The bifacial PV modules generate electricity from the front and back sides, in contrast to monofacial ones, that only generate electricity from the solar radiation on the front side.

1.1. State of the art: bifacial PV

The bifacial photovoltaic modules use bifacial solar cells and have a transparent cover at the back, so they produce electricity using also the radiation received at their backside. The radiation received at the back depends mainly on the ground reflectance (albedo), but also of the heigh of the modules, inclination, modules row-to-row distance, modules row length and some other parameters that may impact the optical scene.

The first pioneering experiences with the development and manufacturing of bifacial PV modules were made in the early 1980s [6]. This was followed by the development of the first calculation models [7]. For a long time, the bifacial PV modules were more expensive than their standard monofacial counterparts, and the additional backside production could not compensate for the higher price. Today, however, bifacial PV modules are finally available at almost the same price per watt peak. They are the most cost-effective PV solution and are becoming the overall best technology for electricity generation [8].

In 2018, a global analysis of the potential gain of bifacial PV systems was conducted [9], which showed that the bifacial gain of bifacial ground-mounted modules at a common albedo of 0.25 is less than 10 % globally. However, by increasing the albedo to 0.5 and elevating the modules 1 m above the ground, the bifacial gain can be increased to 30 %. The final bifacial gain is a combination of the irradiance on the back compared to the irradiance on the front (bifacial ratio) and the PV efficiency of the back compared to the front (bifaciality of the modules). The bifacial ratio (i.e. the radiation received on the back of the module) depends strongly on the albedo (i.e. the ground reflection), but is also influenced by geometric parameters such as the distance between rows, the module height, the module inclination and the row length [10]. As for the operating temperature and its effect on PV production, only when the bifacial ratio exceeds 15 % can the additional heat input cause the bifacial modules to be hotter than their monofacial counterparts, but the energy yield is still much higher [11]. The spectral nature of the albedo is also known to have a significant impact on bifacial PV performance, with back spectral impact observed up to 1.20 for fixed slope systems above green vegetation and up to 0.98 for systems above snow [12].

The use of bifacial PV modules has been proposed not only for utility-scale electricity generation systems, but also for agriculture, water and building environments [8,13]. The bifacial modules have already been proposed for use in buildings in various ways, e.g. vertically mounted in combination with green roofs [14], integrated on the roof to boost power generation in countries with limited land [15] or as solar shading [16]. Chen et al. [17] investigated the integration as skylight and curtain wall as well as the relationship between bifacial gain and internal daylighting.

1.2. State of the art: cool roof

Cool roofs (CR) are highly reflective coatings with a high emissivity in the thermal infrared. They are normally used on building roofs because they lower their temperature compared to corresponding roofs without the coating. They have been shown to significantly reduce the energy required for cooling buildings and the heat island effect in urban environments and can offer economic benefits [18]. It is also known that the energy production of bifacial photovoltaic systems increases when the albedo of the ground is increased. Typical reflectance values for commercial roofing materials range from 0.05 to 0.36, while typical aged reflectance values for cool roofing materials range from 0.55 to 0.65. The thermal emittance for most reported cool roofing materials is typically 0.90 [19].

The usefulness of CR on roofs to improve comfort and reduce energy consumption has been highlighted in many experimental and

theoretical studies. For example [20], in California (USA) studied six types of roofs of commercial buildings and found that increasing the solar reflectance of the roofs by 0.33–0.60, reduced peak temperatures by 33–42 °C and daily energy consumption for cooling by 4 %, 18 % and 52 % in a cold storage warehouse, a school building and a department shop building, respectively. Romeo et al. [21] reported from field measurements that the application of a cool roof coating reduced the cooling load for a 700 m^2 roof by 54 %. Yew et al. [22] reported a large reduction in attic air temperature of about 15 °C compared to a normal roof in Malaysia.

From an economic perspective, the benefits of CRs have been shown to lead to significant savings. In the Mediterranean region, where the present work is located [18], found that a large-scale implementation of cool roofs in Andalusia, in the south of Spain, could potentially save 59 million euros per year in electricity costs, considering only residential buildings with flat roofs that are electrically heated. However, there are significant differences in the economic savings depending on the energy source and the efficiency of the equipment used for air conditioning, as both strongly influence the economic results [23]. If the roof pitch is more than 20°, the cooling effect could be reduced due to the visibility factor to the sky [24].

As a negative aspect, it has been reported that CR tends to increase the consumption of heating energy for buildings in winter [18, 20]. Therefore, efforts have been made to develop a switchable roof reflectance technology [19,25]. It should be considered that the reflectance of CR may decrease by about 20 % in the first two years and stabilises thereafter [18]. However, for an ordinary roof, solar reflectance can be restored to 90 % of the original value by washing, as most of the deterioration is mainly caused by dirt deposits and not by UV or hydrolytic degradation [26].

1.3. Previous experiences combining high reflectance coatings and bifacial in buildings and novelty of this work

Even though there are several cases of bifacial photovoltaic systems on roofs [8], the studies in combination with highly reflective surfaces for buildings are very limited, even though the bifacial panels could benefit from high reflectance surfaces because it increases the radiation received at their backside In the scientific research, there is only one study analysing a cool roof solution in combination with bifacial systems [27,28], but it does not provide information on roof/ground temperature. This lack of literature is also noticed in a recent paper [29], where an interesting analysis of the influence of roof albedo on bifacial PV is performed using artificial neural networks, including the case of CR. The results show that increasing the surface albedo from 0.2 to 0.5 and from 0.2 to 0.8 helps to increase the annual electricity production of bifacial PV by 7.75 % and 14.96 %, respectively. Muehleisen et al. [10] investigated the effects of the common white colour coating in bifacial systems. Initially, a benefit of 17 % was observed for the east-facing panels and 15 % for the west-facing panels, but this decreased to 7 % and 5 %, respectively, after one year due to albedo loss. Al-Sallal et al. [30] used a nano-modified reflective coating that increased the initial albedo by 36.56 % and produced 2.8 % more electricity than bifacial modules above a normal floor and 13.2 % more than monofacial modules. Cavadini et al. [31] modelled the effects of CR for monofacial systems. There is thus a lack of experimental scientific literature on the use of highly reflective surfaces, especially CR, in combination with bifacial modules.

Although there is no scientific information, some commercial initiatives emerged a few years ago. Abolin Co reported in 2012 [32] on the combination of PV and CR using Solyndra's cylindrical PV panels or Sanyo's Double Hit Bifacial modules, one of the few bifacial

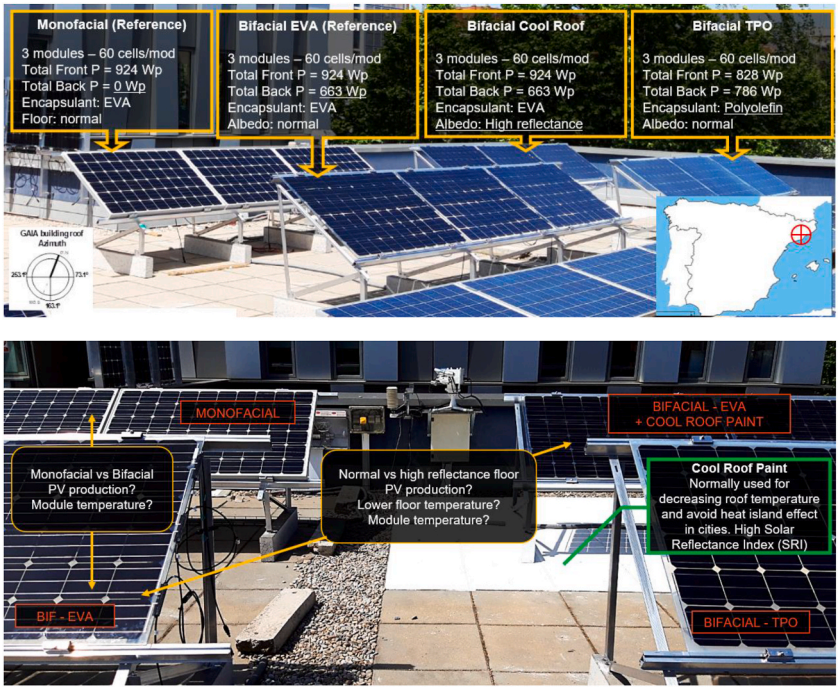

Fig. 1. Images of the four PV systems: monofacial, bifacial above normal floor, bifacial above cool roof coating, and bifacial above normal floor with TPO modules.

modules at that time. They mentioned that using this type of modules in combination with CR could increase the annual energy yield in different European cities by 21–28 % compared to standard PV modules. However, no scientific references were found to confirm such studies. Soprasolar – Soprema and Opsun also mention this possible combination [33,34], but no scientific information was found.

In this sense, the aim of this work is to experimentally demonstrate the combined benefits of cool roof coatings (CR) with bifacial PV systems, that can use the high reflectance properties of the coating to increase the radiation received at the backside and, thus, energy production. Both products have already proven their benefits individually, but their combination could improve the performance of the bifacial system while reducing the building's cooling demand and the heat island effect. As it has been mentioned, the scientific studies combining bifacial photovoltaics and highly reflective surfaces for buildings are very limited, even though could be an interesting and easy solution to implement.

2. Outdoor experimental research

2.1. Description of the test bench

The purpose is to measure the indicators related to the PV production together with indicators of building energy performance. Thus, the testbench comprises four PV systems (Fig. 1), each consisting of three bifacial PV modules connected in series. They are located on the terrace of the GAIA Building of the UPC in the Tarrasa municipality near Barcelona. The four PV systems serve different purposes: (1) monofacial array for reference, (2) bifacial array above the normal floor, (3) bifacial array above Cool Roof coated floor, (4) bifacial array above the normal floor with other types of PV modules. Arrays (1) (2) (3) are made of bifacial modules from JA Solar (JAM60D09 320/BP). Note that the same bifacial modules were also used in the monofacial array, where the back of the module is covered with white opaque vinyl, so that the optical conditions are the same as those of a monofacial PV module, including the gain of the back reflection [35]. Array (4) consists of bifacial modules encapsulated with TPO instead of EVA, with a lower peak power on the front side but a higher bifaciality of the modules (see Table 1). The purpose of array (4) is to evaluate the potential degradation differences between EVA and TPO in a glass-glass configuration [36] and the impact of higher bifaciality as in Ref. [10]. Each PV array is oriented with an azimuth of 163° to the south, tilted 34°, has a ground clearance height of 50 cm and a row-to-row distance of about 3 m. Each PV array is connected to the grid via a single-phase 1.5 kW inverter (SolaX) (Table 2). The test bench has been monitored from April 2020 to November 2021 (both included). When analysing the data, 1 h was used as a time step.

2.2. Description of the monitoring system

The PV array includes several sensors that continuously measure weather and environmental parameters. Fig. 2 shows the plan of the installed sensors, including DNI (direct normal) and GHI radiation pyranometers, air temperature and humidity, wind velocity and direction, radiation at POA (MS40A, 34° inclination), various floor (TF_XX) and module (TC_XX) temperatures and several Si-pyranometers on the back of the modules (ML_XXX). The module temperature is measured with the thermocouples, which are mounted on the back of the glass in the area occupied by the solar cell (instead of in the transparent area). The temperature sensor area is very small, so that a significant effect on backside radiation is not to be expected. Table 6 (in the Appendix) summarises the information about the sensors installed to measure the weather and environmental parameters. The current and voltage sensors are installed before and after the four PV inverters and are summarised in Table 7 in the Appendix section.

The data acquisition (DAQ) process includes the sensors, the signal conditioning circuits, and the analogue-to-digital converters (ADC). The DAQ system consist of two DAQs, one for indoor and one for outdoor use, connected via an Ethernet cable. The cDAQ-9185 offers good performance and is in the Active Phase of the Hardware Life Cycle. The monitoring programme for the PV systems is developed in the LabVIEW environment. Although the time step of data collection is relatively small, the final analysis was based on hourly data. A detailed description of this system can be found in Ref. [37].

2.3. Study of shadows

The surrounding buildings cast shadows on the prototypes in winter. To determine the exact period, a specific analysis of the PV production profiles and with 3D design was carried out.

Fig. 3 shows the PV production profiles of the prototypes on a clear-sky day in December. It can be observed that there are drops in production due to the shadows moving from west to east, so they affect the prototypes at different hours depending on their position. First the drop is observed in B_EVA and Mono, then in B_TPO and B_CR. In the afternoon, a new shadow affects the systems; again, first on B_EVA and Mono, and then on B_CR and B_TPO. Finally, at the end of the day, it seems that Mono works without being shadowed for a while, while others do not.

Fig. 4 shows the PV production profiles of B_TPO and B_EVA at the end of October, when the shadows start to affect the system. During the first three days, there is a shadow that affects B_EVA but not B_TPO. Finally, this shadow also begins to affect B_TPO.

Table 1
PV arrays electrical specifications under STC.

Prototypes	Power Front [Wp]	Power Back [Wp]	Bifaciality	Front Efficiency
Mono	924	0	0 %	21.1 %
B_EVA	924	663	72 %	21.1 %
B_TPO	828	786	95 %	18.9 %
B_CR	924	663	72 %	21.1 %

Table 2
PV inverter specifications, SolaX 1.5 kW

	Parameters	Values
Input/DC	Max. recommended DC power [W]	1650
	Max. input DC voltage [V]	400
	MPPT voltage range [V]	70–380
	Start input/output voltage [V]	60/90
	Number of MPP tracker/strings per MPP tracker	1/1
Output/AC	AC nominal power [W]	1500
	Max. AC power [VA]	1500
	Nominal AC voltage; range [V]	220/230/240; 180~280
	AC grid frequency; range [Hz]	50/60; ±5
	Max. AC current [A]	7.5
	Power factor (full load)	0.8leading ~ 0.8lagging
	Total harmonic distortion (THD)	<1.5 %
	Standby power [W]	<10
Efficiency	MPPT Efficiency [%]	99.9
	Euro Efficiency [%]	96
	Max. Efficiency [%]	97.1

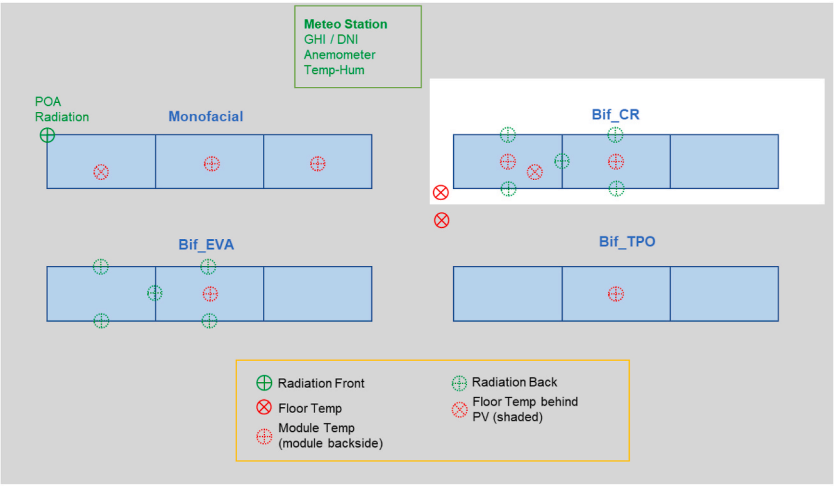

Fig. 2. Sensor plan.

These shadows were also analyzed using 3D modelling. Fig. 5 displays the 3D model created with SketchUp® software to provide a more comprehensive assessment of their location and impact during various times.

3. Results and discussion

The test bench was monitored from April 2020 to November 2021, both inclusive. As previously mentioned, the surrounding buildings cast shadows on the PV prototypes during the winter months. Consequently, the results are presented for either the period without shadows ("Period w/o sh"), which encompasses the entire monitoring period except for November to February, or for a full year from November to October, encompassing the shadowed period as well.

3.1. PV production and performance

PV production and performance were analyzed using PV yield and operational efficiency. The PV yield results were used to compare the relative gains/losses between the different prototypes. Net energy is not a comparable parameter because the prototypes B_EVA, B_CR and Mono use one type of module, while B_TPO uses another with higher bifaciality but lower peak power.

Fig. 6 displays the monthly PV yield of the different prototypes. This yield was calculated considering only the power of the front of the bifacial PV modules and the DC production. To avoid the effect of inverter efficiencies, DC is considered instead of AC. In addition, the monthly irradiation on the 34° plane (POA) is included. The annual results (Table 3) pertain to the period from Nov-20 to Oct-21 (included), while the "period without shadows" includes results from Apr-20 to Oct-20 and from Mar-21 to Oct-21, excluding the period when shadows from surrounding buildings affect the results.

These results show that the highest yield corresponds to the prototype with bifacial modules above the cool roof (B_CR), followed by B_TPO. Regarding the B_CR, the higher reflectance of CR contributes to receive more radiation at the backside of the bifacial modules, so that they can produce more energy. This increased was expected as it is already known from bifacial installations, whose

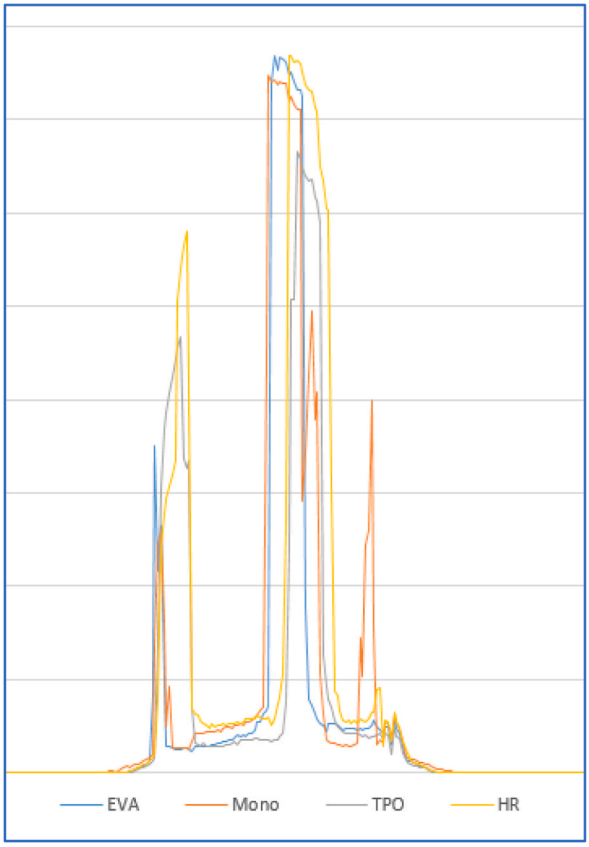

Fig. 3. PV production profile during a clear-sky day in December.

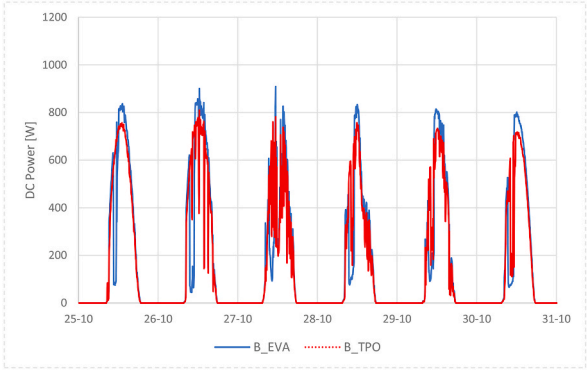

Fig. 4. PV production profiles of B_TPO (red) and B_EVA (blue) prototypes by the end of October. (For interpretation of the references to colour in this figure legend, the reader is referred to the Web version of this article.)

energy production increase depends on ground/floor albedo. Concerning B_TPO, its higher yield is probably caused by its higher bifaciality (backside efficiency compared to front side is higher than in other PV modules), also influenced by the high reflection of the cool roof due to its proximity. The monthly data can be seen in Table 8 in the Appendix.

It is interesting to analyse the yield of the different prototypes and evaluate how the differences might affect PV performance. Fig. 7 shows the relative difference between the prototypes for the entire "Period w/o sh", while Table 9 in the Appendix shows the monthly results. During the "Period w/o sh", the bifacial modules above the normal floor (B_EVA) produced 4.3 % more energy than the corresponding modules without the backside contribution (Mono) due to the additional radiation received at the backside. When the cool roof is used under the bifacial modules (B_CR), the output increases by another 4.1 % compared to the normal floor (B_EVA) due to its higher reflectance. In the aggregate, comparing the bifacial with B_CR floor with conventional monofacial PV system, the overall increase in performance is 8.6 %. For an approximate economic reference, the additional 122 kWh/kWp of B_CR compared to Mono

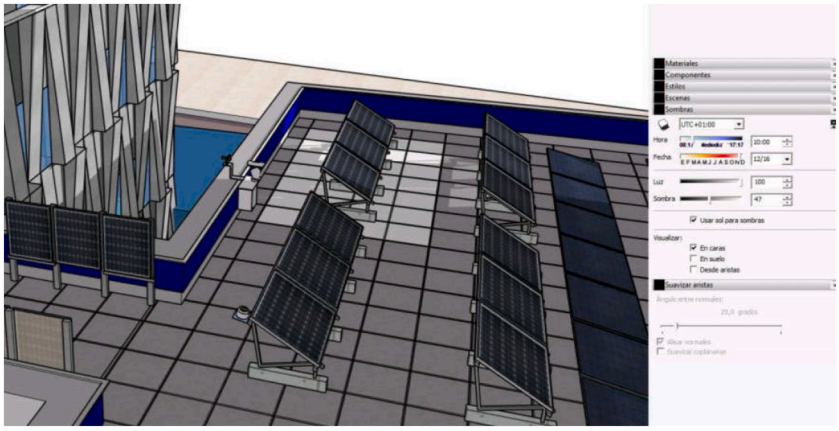

Fig. 5. 3D model for the simulation of shadows using SketchUp®.

Table 3
PV Yield of the prototypes.

	Irradiation POA [kWh/m2]	Yield [kWh/Front kWp]			
		Mono	B_EVA	B_CR	B_TPO
Yearly Nov–Oct	1429	1297	1312	1419	1335
Period w/o sh	2184	2065	2153	2242	2169

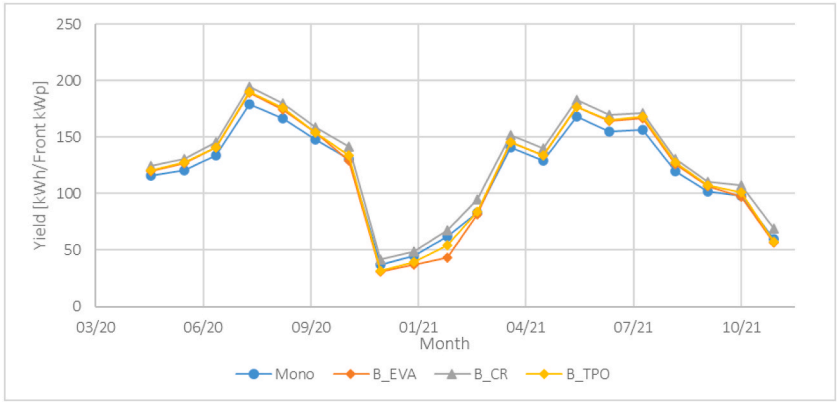

Fig. 6. Monthly PV yield for the whole monitoring period. Shades from November to February, both included. (For interpretation of the references to colour in this figure legend, the reader is referred to the Web version of this article.)

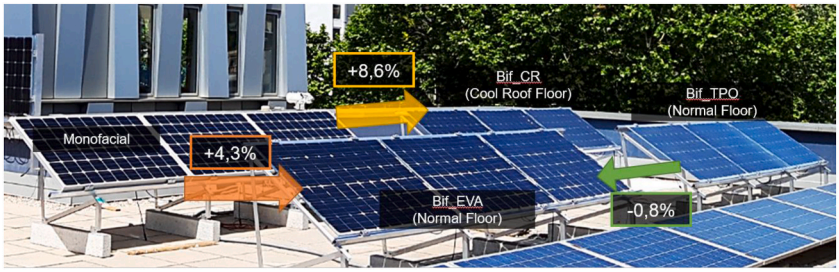

Fig. 7. Yield comparison between the different prototypes. Based on 20 months period without shadows ("w/o sh"). Yield is based on the front peak power only.

would provide 18,3 €/kWp/year (electricity cost of 15c€/kWh). For a family having a 5 kWp installation (1 kWp ≈ 5 m^2 of panels) would means 91,5 €/year.

The B_TPO has a better yield than the B_EVA, although both are bifacial modules above the normal floor. This is because the B_TPO modules contain cells with a measured bifaciality of 95 %, while the bifaciality of B_EVA modules is 72 %; in addition, the proximity of the B_TPO modules to the cool roof could slightly affect the results. It should be noted that the additional power of the rear side is not considered in the yield results, which are based only on the power of the front side (and the bifaciality of the PV cells).

Another interesting parameter is the operating efficiency (η_f or η_{tot} as per [38]) defined in Equation (1), that provides the efficiency of the module in operating conditions (for instance, including the efficiency reduction due to higher operating temperature):

$$\eta_{op} = P_{DC}/G \bullet S \quad \text{Equation 1}$$

Where G is the incident solar radiation (W/m^2), S is the active PV field area and P_DC is the generated electrical PV power in DC. For monthly data (e.g. monthly operating efficiency), the power is replaced by the monthly DC energy and G by the monthly irradiance.

According to this definition, the performance ratio (PR) in DC of the PV prototypes would be as described in Equation (2):

$$PR_{DC} = \eta_{op}/\eta_{STC} \quad \text{Equation 2}$$

Table 4 illustrates the operational efficiency of the prototypes compared to the front STC efficiency of the modules (monthly data in Table 10). It includes the PR of the period with shade (year Nov–Oct) and the PR of the period without shade (*Period w/o sh*). The annual PR is summarised in Fig. 8. The PR does not incorporate inverter losses, as it is based on DC data.

The best result is achieved by the bifacial above CR floor (B_CR), whose operational efficiency surpasses the front efficiency measured in STC. This implies that the additional production from the bifacial setup compensates for the combined system losses of the corresponding monofacial system, resulting in a PR greater than 100 %. The two bifacial prototypes above the normal floor, B_EVA and B_TPO, have similar efficiency to STC conditions, i.e. nearly 100 % PR. The Mono case demonstrates the efficiency and PR of ordinary PV systems, both for the period with shade and the period without shade. From a monthly perspective, there is a slight decrease in efficiency in summer, caused by the higher operating temperature of the modules.

3.2. Operating temperature of the PV modules

The operating temperature of the PV modules can vary depending on the absorbed radiation. Since the modules operate under different optical conditions, it is interesting to analyse this parameter. The temperature of the solar cell affects the PV efficiency, i.e. the higher the temperature, the lower the efficiency. Recent studies suggest that bifacial PV modules usually operate at lower temperatures unless the bifacial ratio is higher than 15 % [11], but other studies present opposing findings [39]. Even though the current experiment is not fully focused on this analysis, it is interesting to measure and share this information with the community.

Fig. 9 shows the average operating temperature of the modules for the different months. Fig. 10 shows the annual averages in one picture and the whole data is given in Table 11 in the Appendix. In addition, Table 5 examines the temperature differences among the most significant cases.

The bifacial modules above normal floor (B_EVA) appear to operate at a slightly higher temperature than the monofacial ones (+0.6 °C), particularly during months with high radiation. The bifacial system above the cool roof (B_CR) operates at an average temperature 1.6 °C higher than its counterpart above the normal floor (B_EVA), especially during months with high radiation. The average temperature of B_EVA prototype is +0.7 °C higher than that of B_TPO, although both are bifacial modules above the normal floor, and the PV efficiency of B_EVA is higher. This discrepancy could be attributed to various factors, such as a differences in the prototype's position on the terrace, the location and attachment of the thermocouple, or a combination of both.

In the case of Mono and B_CR, two additional thermocouples (Mono_ext and B_CR_ext) are located in the first module of the row instead of in the middle (second) module. This is done to assess potential temperature differences along the row. The results indicate that the average temperature of B_CR_ext is 0.4 °C lower than that of B_CR, while that of the Mono_ext is 0.4 °C higher. These differences are smaller than the uncertainty of the thermocouples. Thus, there is no clear conclusion on the potential temperature variations along the PV row, which is expected since it consists of only three modules.

3.3. Backside radiation

Several irradiation sensors are mounted on the back of the bifacial prototypes B_EVA and B_CR. The purpose is to measure the

Table 4
Operating efficiency of the prototypes.

	Operational Efficiency [%]			
	Mono	B_EVA	B_CR	B_TPO
Yearly Nov–Oct	19.1 %	19.4 %	20.9 %	17.7 %
Period w/o sh	**19.9 %**	**20.8 %**	**21.6 %**	**18.8 %**
Eff STC	21.1 %	21.1 %	21.1 %	18.9 %
Δ Eff	**−1.2 %**	**−0.3 %**	**0.6 %**	**−0.1 %**
PR w Sh	90.8 %	91.8 %	99.3 %	93.4 %
PR w/o Sh	**94.5 %**	**98.6 %**	**102.6 %**	**99.3 %**

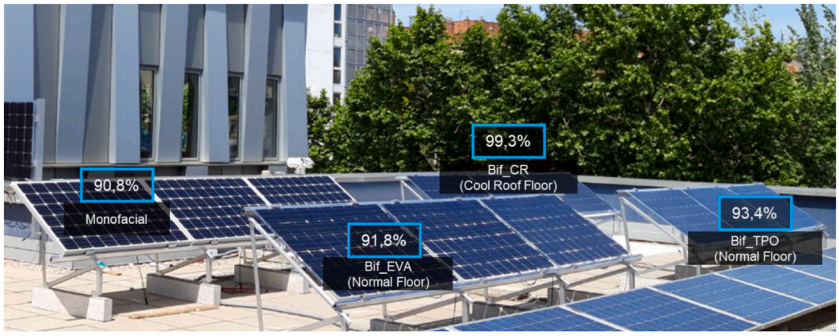

Fig. 8. PR_{DC} of the prototypes. Based on 1 year including shaded period.

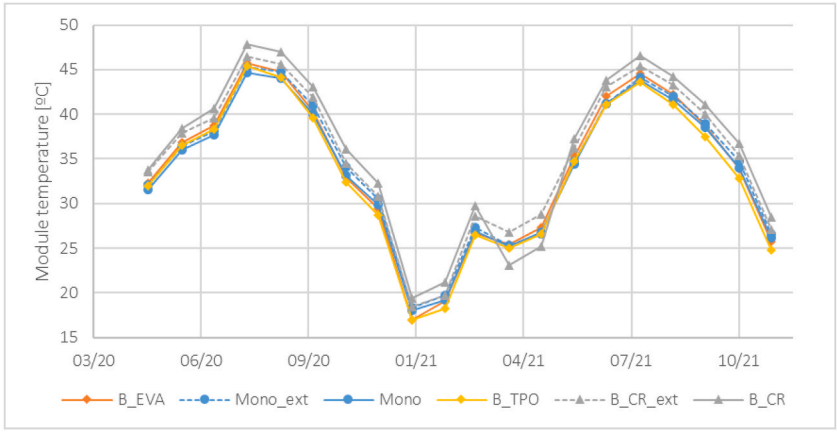

Fig. 9. Average monthly operating temperature of the PV modules with POA radiation higher than 100 W/m^2.

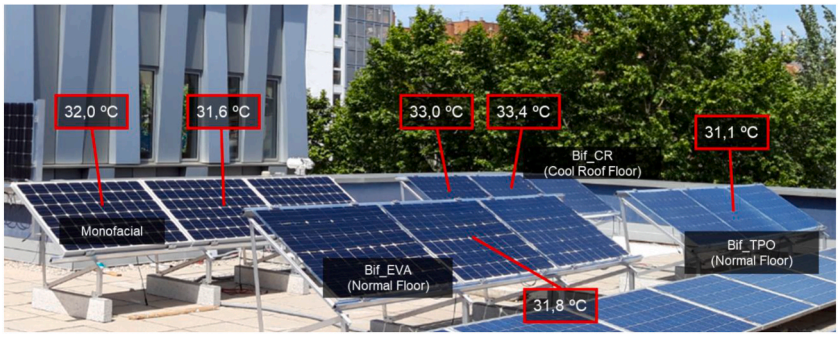

Fig. 10. Yearly operating temperature of the PV modules. Data with POA radiation higher than 100 W/m^2 only. Red lines indicate the position of the sensors at the back side of PV panels. (For interpretation of the references to colour in this figure legend, the reader is referred to the Web version of this article.)

Table 5
Differences of average operating temperatures.

	EVA-Mono	CR - EVA	EVA-TPO	Mono-Mono_ext	HR-HR_ext
Period w/o sh	0.2	1.6	0.7	−0.3	0.4
Yearly Nov–Oct	0.6	1.6	0.7	−0.4	0.4

irradiance of the back surface in different positions, as this impacts on the performance of bifacial panels and is expected to be linked with the floor reflectance. Their positions are described in Fig. 2 and Table 6. The main indicator is the bifacial ratio (BR), i.e. the ratio between the irradiance received on the back side of the module and the irradiance received on the front side.

Table 12 and Table 13 in the Appendix show the monthly BR measured by the sensors in prototypes B_EVA (normal floor) and B_CR (cool roof), while Fig. 11 summarises them in one picture. Due to its definition, the BR is strongly (but not only) linked to the ground reflection (albedo).

The average annual bifacial ratio of B_EVA is 7.4 %, while for B_CR it is 13.7 %. A significant portion of the radiation is, therefore, received on the backside, especially in the case of bifacial PV modules above the cool roof coated floor. For reference, bifacial ratio of large bifacial PV plants are about 4–7% for common ground albedos of 15–20 %, but it is known that BR is increased when albedo is higher.

According to this backside radiation and the bifaciality of the modules, the theoretical bifacial gain of B_EVA would be 7.4 %*72 % = 5.33 %, while for B_CR it would be 13.7 %*72 % = 9.86 %. However, the measured gain is 4.3 % for B_EVA (vs Mono) and 8.6 % for B_CR (vs Mono). The difference could be attributed to several reasons like the reflection of the opaque white backsheet of the monofacial module, which normally increases the production by about 1–2% [35]; the limited production due to the lower BR point; and the higher operating temperature of the B_CR. Concerning the back reflection of the monofacial module, it should be noted that this was chosen intentionally to make a comparison with a common monofacial module alternative that also includes this gain.

When comparing the different sensors in the two prototypes B_EVA and B_CR, we can observe that the sensors in the lower part of the modules receive more radiation. Also, in both cases, the least radiation is received by the sensors in the middle and top left. In the case of B_CR, the upper left sensor receives significantly less radiation, possibly due to its lower viewing angle of the cool roof.

During the monitoring period, the cold roof was not normally cleaned intentionally, except by rain or natural events. However, in early September 2021, the cool roof was cleaned to assess the impact of dirt accumulation. Comparing the bifacial ratio of Sep-21 and Oct-21 with the same months of the previous year, we find that there is an increase of about 0.8–1% points in BR, so it seems that this could be the effect of cleaning. However, there is also an increase from Aug-20 to Aug-21, although the floor was still dirty in Aug-21. The profiles of production and of BR show no remarkable increase after cleaning on these days. Therefore, there is no clear indication of what the effect of cleaning the cool roof might be, but probably frequent cleaning is not necessary.

In general, the differences between the radiations received at different points (Δmax in Table 12 and Table 13) at B_EVA are 1–3% points. In the case of B_CR, the differences are between 2 and 5% points. Both are relevant quantities, considering that BR is 7.4 % and 13.7 %. It can thus be seen that the back irradiation is not homogeneous. Homogeneity could be improved by increasing the height of the modules above the floor, but this could increase the complexity and the demands on the structure.

3.4. Floor temperature

Prototype B_CR is designed not only to increase PV production, but also to lower the floor temperature, thus reducing the building's cooling requirements in summer. The CR coating used under prototype B_CR is designed to prevent the building roofs from heating up by reflecting as much solar radiation as possible and having a high emissivity in the thermal infrared range.

Temperatures on the normal and cool roof were measured in an unshaded area and a shaded area directly under the PV panels. The aim was to measure the effects of the cool roof coating, but also the effects of the PV shading on the floor temperature. Figs. 12 and 13 show the monthly and seasonal results, while the data can be found in Table 14 and Table 15 in the Appendix.

In winter, the temperature of the floor covered with a cool roof coating is 1.4 °C lower than that of the conventional floor due to lower absorption of sun radiation. The temperature of the floor under the PV panels (shaded, sh) is also very similar in winter in both the Normal and B_CR cases. The average temperature of the shaded area in winter is 0.9 °C higher than Normal and 2.2 °C higher than B_CR. This means that the PV panels contribute to a higher temperature of the roof n winter, thus reducing heating consumption. This is probably because they reduce heat exchange through long-wave radiation, especially during the night. However, it should be noted that the floor with cool roof only (without the PV panels) will be slightly colder than normal floor, so it may slightly increase the heating needs. This fact was already known from previous studies [18,20] and the reason why CRs are recommended for climates without hard winter.

During the summer, the temperature of the exposed floor with B_CR is 3.8 °C lower than that of the normal floor, which is a significant temperature decrease. During this period, the temperature of the floor below the PV panels is very similar for both Normal and B_CR. This temperature is significantly lower than the temperature of the exposed areas, especially the exposed normal floor

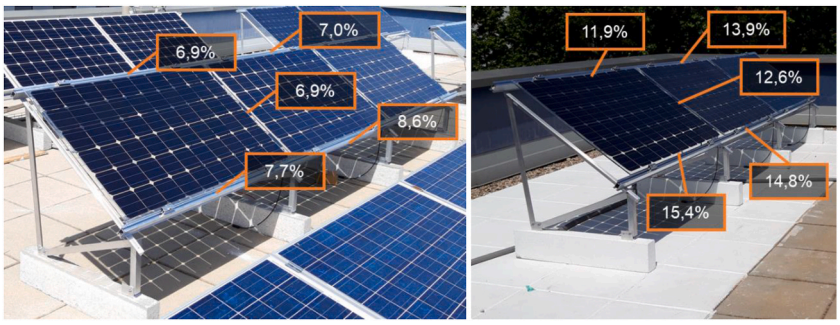

Fig. 11. Yearly bifacial ratio measured at different points of system backside. Orange lines indicate the position of the sensors at the back side of PV panels. (For interpretation of the references to colour in this figure legend, the reader is referred to the Web version of this article.)

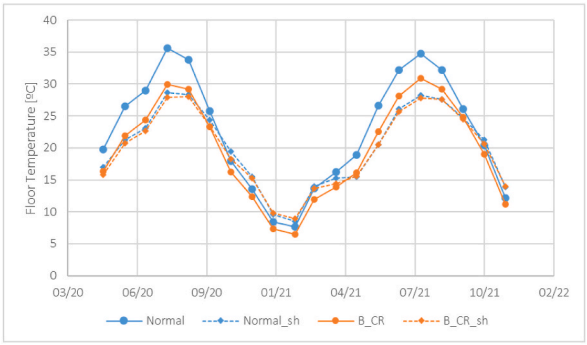

Fig. 12. Monthly average floor temperature of normal floor and cool roof coated floor, in a shaded area below PV modules (sh) and an exposed non-shaded area.

Fig. 13. Average seasonal floor temperature of the normal floor and the cool roof coated floor, in a shaded area below PV modules (sh) and an exposed non-shaded area.

(−5 °C). So, during the summer, there is a significant decrease in the floor temperature due to B_CR, especially in the exposed areas. In the case of the normal floor, there is a significant reduction due to shading from the PV panels.

In summary, the use of cool roof coatings for bifacial PV systems with a large distance between rows (low Ground Coverage Ratio, GCR) could be a good solution, especially in the areas exposed to radiation. Moreover, the large distance between rows could favour the bifacial gain. When the distance between rows is small (high GCR), the benefits of the cool roof coating are lower due to less floor reduction and lower bifacial gain, but it can still be attractive.

4. Conclusions

In this paper, several bifacial PV systems, each with a capacity of approximately 1 kW, were tested on a terrace in a Mediterranean climate. The bifacial PV technology demonstrated an increase in PV production (4–4.5 %) compared to the monofacial systems, attributable to the additional radiation on the back of the modules. This was measured in two prototypes, one made with commercial modules laminated with EVA and the other with TPO laminated modules.

When a cool roof coating (CR) is used beneath the bifacial modules, PV production can be substantially boosted (+8.6 %) compared to the monofacial solution, meaning an economic benefit about 18,3 €/kWp/year (1 kWp ≈ 5 m^2 of panels). Moreover, the CR coating can help reduce floor temperatures in unshaded areas during summer (−3.8 °C), potentially leading to significant energy savings in cooling the building. The use of cool roof coating holds particular appeal for PV systems with large row spacing, where a substantial portion of the floor is exposed to sunlight. Not only does it lower floor temperatures, but it also enhances bifacial gains. However, it is worth noting that the use of CR without PV panels may slightly decrease floor temperature in winter, which could have a negative impact on heating consumption, particularly in cold winter regions and warrants further analysis.

The PV-only systems (without CR) can still contribute to reduce the energy demand of the building by better controlling the floor temperature. In winter, the temperature of the normal floor is 0.9 °C higher with a PV system compared to without, while in summer, it is 5 °C lower. Rooftop PV systems can thus positively influence the thermal performance of the building, even if they are treated as BAPV, a phenomenon previously studied [5] but was also observed in the present work.

Backside irradiance on bifacial modules exhibits non-uniformity, leading to potential mismatch losses between different module points. The lower area receives the highest radiation, whereas the top, near the corners, experiences the lowest.

No significant differences or events were observed between bifacial modules laminated with TPO and those commonly using EVA. Nevertheless, a longer period of analysis might be needed to evaluate the differential aging of the encapsulations.

Finally, the operating temperatures of bifacial modules seem to be somewhat higher. However, this fact does not have a significant effect and does not prevent the higher performances.

Both bifacial and CR technologies have already individually demonstrated their positive effects on energy and economics. However, this work illustrates that bifacial technology can also benefit from CR coatings, enhancing the overall impact from economic and energy standpoints. The CR could be applied to the floor of existing bifacial PV rooftop installations or incorporated into new installations. It is an already available market product with reasonable costs that offers dual advantages: increased energy yield and reduced building cooling consumption, both yielding economic benefits.

Author statement

Daniel Valencia-Caballero: Conceptualization, Methodology, Validation, Formal Analysis, Investigation, Resources, Writing – Original Draft, Visualization; **Salim Bouchakour**: Methodology, Software, Validation, Investigation, Resources, Data Curation, Writing – Original Draft, Visualization; **Alvaro Luna**: Resources, Writing - Review & Editing, Supervision, Project administration, Funding acquisition; **Borja Garcia-Marco**: Investigation, Visualization; **Ana Huidobro**: Project administration, Funding acquisition; **Iván Flores-Abascal**: Writing - Review & Editing, Supervision; **Asier Sanz**: Writing - Review & Editing, Supervision; **Eduardo Román**: Writing - Review & Editing, Supervision, Project administration, Funding acquisition.

Declaration of competing interest

The authors declare that they have no known competing financial interests or personal relationships that could have appeared to influence the work reported in this paper.

Data availability

Data will be made available on request.

Acknowledgements

This work was supported by the SUDOKET SOE2/P1/E0677 project funded by FEDER of the EU under the Interreg-Sudoe program.

Appendix

Table 6
List of weather and environmental sensors

Measured variables	Sensors			
	Type	Reference	Reference in the plan	Error
GHI	Pyranometer.	EKO, MS-80A	MS80A	<0.5 %
DNI	Sun-tracker	EKO, STR-21G	–	–
	Pyrheliometer	EKO, MS-65	MS65	<0.5 %
POA irradiance	Pyranometer	EKO, MS-40A	MS40A	<1.5 %
Rear irradiance Normal floor	5 × Si-pyranometer	EKO, ML-01	ML_745 (top-left) ML_741 (top-right) ML_742 (middle) ML_743 (bottom-left) ML_813 (bottom-right)	< ±2 %
Rear irradiance High reflective floor	5 × Si-pyranometer	EKO, ML-01	ML_811 (top-left) ML_744 (top-right) ML_740 (middle) ML_814 (bottom-left) ML_812 (bottom-right)	
PV module temperature, TC	7 × Thermocouple	RS Components, Type K	TC_S1_CH7 TC_S22_CH9 TC_S21_CH2 TC_S3_CH6 TC_S42_CH12 TC_S41_CH1 TC_S5_CH8	±0.75 %
Floor temperature, TF	4 × Thermocouple	RS Components, Type K	TF_CH4 TF_HR_CH0 TF_S2_CH5 TF_S4_CH3	
Humidity and Ambient temperature	Moisture meter	HYGRASGARD® KFTF-I	KFTF-I Tamb	±1.8 % ±2 %
Wind velocity and direction	Anemometer	Disibeint Electronic, SVR 40	SVR40	±0.5 m/s

Table 7
List of electrical sensors

Measured variables	Sensors			
	Type	Reference	Reference in the plan	Sensitivity/Output Range/Error
DC voltage	4 × Transducer	Magnelab, DVT-1000-V05	Vdc_BF Vdc_Mono Vdc_BF-TPO Vdc_BF_HR	Range: 0 … 1000 V. Output: 0 … 5 VDC. ±1 %
DC current	4 × Transducer	Magnelab, HCT-0010-010	Idc_BF Idc_Mono Idc_BF-TPO Idc_BF_HR	Range: 0 … 10 A. Output: ±4 VDC. ±1 %
AC voltage	3 × TRMS voltage isolator converter	SENECA, Z-204-1	Vac_ph1 Vac_ph2 Vac_ph3	Range: 0 … 350 VAC. Output: 0 … 10VDC.
AC current	4 × Transducer	Magnelab, DCT-0010-10	Iac_BF Iac_Mono Iac_BF-TPO Iac_BF_HR	Range: 0 … 10A. Output: 0 … 5VDC. ±1 %

Table 8
PV Yield of the prototypes. With *, period with shadows excluded from "Period w/o sh"

	Irradiation POA [kWh/m2]	Yield [kWh/Front kWp]			
		Mono	B_EVA	B_CR	B_TPO
abr-20	119	116	120	124	120
may-20	128	121	127	131	127
jun-20	134	134	141	146	141
jul-20	195	179	189	195	190
ago-20	181	167	175	180	176
sep-20	157	148	154	159	154
oct-20	134	130	129	142	134
*nov-20	75	37	31	42	32
*dic-20	59	45	38	49	39
*ene-21	74	62	44	68	54
*feb-21	85	83	82	95	84
mar-21	143	141	145	152	146
abr-21	134	129	134	140	134
may-21	179	168	177	183	177
jun-21	167	155	164	170	165
jul-21	174	157	166	171	168
ago-21	130	120	126	131	127
sep-21	107	102	106	111	107
oct-21	102	98	97	107	101
*nov-21	63	60	56	69	57
Yearly Nov-Oct	1429	1297	1312	1419	1335
Period w/o sh	2184	**2065**	**2153**	**2242**	**2169**

Table 9
PV Yield comparison between the prototypes. With *, period with shadows excluded from "Period w/o sh".

	PV Yield comparison			
	B_EVA vs Mono	CR vs Mono	CR vs B_EVA	B_EVA vs B_TPO
abr-20	3.2%	7.1%	3.8%	-0.4%
may-20	5.2%	8.3%	2.9%	-0.2%
jun-20	5.2%	8.8%	3.4%	0.0%
jul-20	5.8%	9.0%	3.1%	-0.6%
ago-20	5.0%	8.1%	3.0%	-0.8%
sep-20	4.0%	6.9%	2.8%	0.0%
oct-20	-0.9%	8.6%	9.6%	-3.4%
*nov-20	-15.5%	12.4%	32.9%	-0.8%
*dic-20	-16.6%	9.1%	30.7%	-5.0%
*ene-21	-29.8%	9.3%	55.6%	-19.3%
*feb-21	-1.7%	13.5%	15.5%	-2.8%
mar-21	3.3%	8.0%	4.5%	0.0%
abr-21	3.9%	8.4%	4.4%	0.0%
may-21	5.4%	9.0%	3.5%	0.1%
jun-21	5.8%	9.5%	3.5%	-0.6%
jul-21	6.2%	9.4%	3.0%	-1.0%
ago-21	5.4%	9.1%	3.4%	-0.8%
sep-21	4.1%	8.5%	4.3%	-0.7%
oct-21	-0.6%	9.7%	10.4%	-4.0%
*nov-21	-5.7%	15.4%	22.3%	-2.0%
Period w/o sh	**4.3%**	**8.6%**	**4.1%**	**-0.8%**

Table 10
Operational efficiency of the prototypes. With *, period with shadows excluded from "Period w/o sh"

	Operational Efficiency [%]			
	Mono	B_EVA	B_CR	B_TPO
abr-20	20.6%	21.3%	22.1%	19.1%
may-20	19.9%	21.0%	21.6%	18.8%
jun-20	21.0%	22.1%	22.9%	19.8%
jul-20	19.3%	20.4%	21.1%	18.4%
ago-20	19.4%	20.4%	21.0%	18.4%
sep-20	19.9%	20.7%	21.3%	18.5%
oct-20	20.5%	20.3%	22.3%	18.8%
*nov-20	10.3%	8.7%	11.6%	7.9%
*dic-20	16.0%	13.3%	17.4%	12.6%
*ene-21	17.6%	12.4%	19.3%	13.8%
*feb-21	20.8%	20.4%	23.6%	18.8%
mar-21	20.7%	21.4%	22.4%	19.2%
abr-21	20.4%	21.2%	22.1%	19.0%
may-21	19.8%	20.9%	21.6%	18.7%
jun-21	19.6%	20.7%	21.5%	18.7%
jul-21	19.0%	20.2%	20.8%	18.3%
ago-21	19.4%	20.5%	21.2%	18.5%
sep-21	20.0%	20.9%	21.8%	18.8%
oct-21	20.4%	20.2%	22.3%	18.9%
*nov-21	20.1%	19.0%	23.2%	17.4%
Yearly Nov-Oct	19.1%	19.4%	20.9%	17.7%
Period w/o sh	**19.9%**	**20.8%**	**21.6%**	**18.8%**
Eff STC	21.1%	21.1%	21.1%	18.9%
Δ Eff	**-1.2%**	**-0.3%**	**0.6%**	**-0.1%**
PR w Sh	90.8%	91.8%	99.3%	93.4%
PR w/o Sh	**94.5%**	**98.6%**	**102.6%**	**99.3%**

Table 11
Average operating temperature of the PV modules with POA radiation higher than 100 W/m^2. With *, period with shadows excluded from "Period w/o sh"

	B_EVA	Mono_ext	Mono	B_TPO	B_CR_ext	B_CR
abr-20	32.3	32.0	31.5	32.0	33.6	33.8
may-20	36.9	36.4	36.0	36.5	37.9	38.4
jun-20	38.8	38.1	37.7	38.3	39.5	40.6
jul-20	45.8	45.3	44.7	45.4	46.5	47.9
ago-20	44.7	44.7	44.0	44.2	45.6	47.0
sep-20	40.4	41.0	40.0	39.6	41.9	43.1
oct-20	32.9	34.1	33.1	32.4	34.6	36.1
*nov-20	29.5	30.5	29.9	28.7	30.8	32.3
*dic-20	17.0	18.3	18.0	16.9	18.4	19.4
*ene-21	19.0	19.7	19.2	18.2	19.7	21.2
*feb-21	26.6	27.3	26.9	26.5	28.6	29.8
mar-21	25.4	25.4	25.2	25.0	26.8	23.1
abr-21	27.3	26.6	26.8	26.6	28.8	25.2
may-21	35.2	34.8	34.4	34.7	36.3	37.3
jun-21	42.0	41.2	41.1	41.0	43.1	43.8
jul-21	44.5	44.1	43.8	43.6	45.4	46.6
ago-21	42.2	42.0	41.7	41.1	43.3	44.2
sep-21	38.8	39.0	38.5	37.5	40.0	41.1
oct-21	33.9	34.7	34.0	32.8	35.3	36.7
*nov-21	25.8	26.6	26.1	24.7	27.1	28.5
Period w/o sh	**37.4**	**37.3**	**36.8**	**36.7**	**38.6**	**39.0**
Yearly Nov-Oct	**31.8**	**32.0**	**31.6**	**31.1**	**33.0**	**33.4**

Table 12
Backside irradiance gain compared to frontside POA irradiance (bifacial ratio, BR). Normal floor (B_EVA). With *, period with shadows excluded from "Period w/o sh". See sensors in Fig. 2.

	B_EVA ML_741	B_EVA ML_742	B_EVA ML_743	B_EVA ML_745	B_EVA ML_813	Mean	Δmax
*abr-20	15.6%	15.8%	17.9%	15.6%	19.5%	16.9%	
*may-20	16.0%	16.2%	20.1%	16.6%	21.3%	18.1%	
jun-20	7.1%	7.2%	8.9%	7.4%	9.5%	8.0%	2.4%
jul-20	7.1%	7.0%	8.6%	7.1%	9.2%	7.8%	2.2%
ago-20	7.2%	7.1%	8.0%	6.9%	8.7%	7.6%	1.8%
sep-20	6.9%	6.9%	6.9%	6.4%	7.7%	7.0%	1.3%
oct-20	6.3%	6.5%	6.3%	6.2%	7.2%	6.5%	1.0%
*nov-20	6.9%	7.1%	7.4%	7.3%	8.5%	7.4%	1.6%
*dic-20	6.6%	6.9%	7.6%	7.2%	8.5%	7.4%	1.9%
*ene-21	6.2%	6.5%	6.9%	6.6%	7.9%	6.8%	1.7%
*feb-21	6.5%	6.6%	6.7%	6.5%	7.7%	6.8%	1.2%
mar-21	6.6%	6.6%	6.6%	6.1%	7.5%	6.7%	1.4%
abr-21	6.7%	6.5%	7.1%	6.3%	8.0%	6.9%	1.7%
may-21	6.9%	6.6%	8.0%	6.7%	8.8%	7.4%	2.2%
jun-21	7.2%	7.0%	8.8%	7.4%	9.7%	8.0%	2.7%
jul-21	7.5%	7.1%	8.7%	7.3%	9.6%	8.0%	2.5%
ago-21	7.8%	7.4%	8.4%	7.4%	9.4%	8.1%	2.0%
sep-21	7.8%	7.5%	7.7%	7.1%	8.7%	7.7%	1.6%
oct-21	7.1%	7.0%	6.9%	6.7%	8.0%	7.2%	1.3%
*nov-21	7.0%	6.9%	7.1%	7.0%	8.3%	7.3%	1.4%
Period w/o sh	7.1%	6.9%	7.8%	6.9%	8.7%	**7.5%**	1.8%
Yearly Nov-Oct	7.0%	6.9%	7.7%	6.9%	8.6%	**7.4%**	1.7%

Table 13
Backside irradiance gain compared to frontside POA irradiance (bifacial ratio, BR). Cool roof (B_CR) floor. With *, period with shadows excluded from "Period w/o sh". See sensors in Fig. 2.

	B_CR ML_740	B_CR ML_744	B_CR ML_811	B_CR ML_812	B_CR ML_814	Mean	Δmax
*abr-20	31.8%	34.7%	29.0%	38.1%	40.2%	34.8%	
*may-20	34.3%	38.1%	29.4%	36.9%	39.2%	35.6%	
jun-20	15.1%	17.0%	13.1%	15.1%	15.8%	15.2%	3.9%
jul-20	14.1%	15.8%	12.2%	14.3%	15.1%	14.3%	3.6%
ago-20	13.1%	14.3%	11.7%	14.8%	15.5%	13.9%	3.8%
sep-20	11.5%	12.3%	11.3%	15.2%	15.6%	13.2%	4.3%
oct-20	10.6%	11.3%	11.2%	14.6%	14.7%	12.5%	4.1%
*nov-20	12.1%	12.9%	12.0%	14.1%	14.6%	13.1%	2.5%
*dic-20	11.6%	12.6%	10.8%	11.7%	12.7%	11.9%	1.8%
*ene-21	10.4%	11.3%	10.2%	11.6%	12.2%	11.2%	2.0%
*feb-21	12.3%	13.3%	13.3%	17.1%	17.4%	14.7%	5.1%
mar-21	11.6%	12.7%	12.0%	16.2%	16.9%	13.9%	5.2%
abr-21	12.5%	13.9%	11.9%	15.3%	16.1%	13.9%	4.2%
may-21	13.4%	15.1%	11.9%	14.3%	15.2%	14.0%	3.4%
jun-21	14.1%	15.9%	12.2%	14.3%	15.1%	14.3%	3.7%
jul-21	13.4%	15.1%	11.6%	14.1%	14.9%	13.8%	3.5%
ago-21	13.1%	14.5%	11.8%	14.9%	15.6%	14.0%	3.8%
sep-21	12.1%	13.2%	12.0%	16.2%	16.6%	14.0%	4.5%
oct-21	11.3%	12.2%	12.0%	15.7%	15.8%	13.4%	4.5%
*nov-21	12.0%	13.2%	12.5%	15.4%	15.5%	13.7%	3.5%
Period w/o sh	12.9%	14.2%	11.9%	14.9%	15.5%	**13.9%**	3.6%
Yearly Nov-Oct	12.6%	13.9%	11.9%	14.8%	15.4%	**13.7%**	3.6%

Table 14
Average floor temperature

	Normal	Normal_sh	B_CR	B_CR_sh
abr-20	19.8	17.0	16.3	15.8
may-20	26.5	21.2	21.9	20.7
jun-20	28.9	23.1	24.3	22.6
jul-20	35.7	28.6	29.9	27.9
ago-20	33.8	28.4	29.2	28.0
sep-20	25.8	24.3	23.3	23.4
oct-20	18.0	19.4	16.2	18.3
nov-20	13.6	15.5	12.4	15.3
dic-20	8.4	9.6	7.4	9.9
ene-21	7.6	8.6	6.5	8.9
feb-21	13.6	14.0	11.9	13.7
mar-21	16.2	15.3	13.8	14.4
abr-21	18.9	15.5	16.1	15.6
may-21	26.6	20.5	22.5	20.5
jun-21	32.2	26.1	28.1	25.6
jul-21	34.8	28.3	30.9	27.8
ago-21	32.2	27.6	29.2	27.6
sep-21	26.0	24.7	24.8	24.5
oct-21	20.5	21.3	19.0	20.6
nov-21	12.2	13.8	11.2	13.9
Winter (1,2,3,11,12)	**11.9**	**12.8**	**10.5**	**12.7**
Summer (5,6,7,8,9)	**30.2**	**25.3**	**26.4**	**24.9**

Table 15
Differences in average floor temperature. CR=Cool Roof, N=Normal floor, Sh = Shaded area.

	CR - N	CR_Sh - N_Sh	N - N_Sh	CR - CR_Sh
abr-20	-3.5	-1.2	2.8	0.5
may-20	-4.6	-0.5	5.3	1.2
jun-20	-4.6	-0.5	5.8	1.7
jul-20	-5.7	-0.7	7.0	2.0
ago-20	-4.6	-0.4	5.4	1.3
sep-20	-2.5	-0.9	1.5	-0.1
oct-20	-1.8	-1.1	-1.4	-2.1
nov-20	-1.2	-0.2	-2.0	-2.9
dic-20	-1.0	0.3	-1.2	-2.5
ene-21	-1.2	0.3	-0.9	-2.4
feb-21	-1.7	-0.3	-0.3	-1.8
mar-21	-2.4	-0.9	0.9	-0.6
abr-21	-2.7	0.1	3.4	0.5
may-21	-4.1	0.0	6.1	2.0
jun-21	-4.1	-0.5	6.1	2.5
jul-21	-3.8	-0.5	6.5	3.2
ago-21	-2.9	0.0	4.6	1.6
sep-21	-1.3	-0.3	1.3	0.3
oct-21	-1.4	-0.7	-0.8	-1.6
nov-21	-1.0	0.1	-1.7	-2.8
Winter (1,2,3,11,12)	**-1.4**	**-0.1**	**-0.9**	**-2.2**
Summer (5,6,7,8,9)	**-3.8**	**-0.4**	**5.0**	**1.6**

References

[1] United Nations Environment Programme, 2022 Global Status Report for Buildings and Construction: towards a Zero-Emission, Efficient and Resilient Buildings and Construction Sector, 2022. Nairobi.

[2] D. Valencia-Caballero, Y.-B. Assoa, W. Cambarau, D. Therme, A. Sanz, F. Burgun, I. Flores-Abascal, E. Román-Medina, Performance analysis of a novel building integrated low concentration photovoltaic skylight with seasonal solar control, J. Build. Eng. (2022), 104687, https://doi.org/10.1016/J.JOBE.2022.104687.

[3] IEC TC 82, ISO TC 160, IEC 63092-1 - Photovoltaics in Buildings - Part 1: Requirements for Building-Integrated Photovoltaic Modules, 2020.

[4] M.M. Fouad, L.A. Shihata, A.H. Mohamed, Modeling and analysis of Building Attached Photovoltaic Integrated Shading Systems (BAPVIS) aiming for zero energy buildings in hot regions, J. Build. Eng. 21 (2019) 18–27, https://doi.org/10.1016/j.jobe.2018.09.017.

[5] M. Fischer, M. Woodhouse, S. Herritsch, J. Trube, International Roadmap for Photovoltaic (ITRPV) - 2021 Results, 2022. Frankfurt am Main.

[6] J. Eguren, F. Martínez-Moreno, P. Merodio, E. Lorenzo, First bifacial PV modules early 1983, Sol. Energy 243 (2022) 327–335, https://doi.org/10.1016/j.solener.2022.08.002.

[7] E. Lorenzo, On the historical origins of bifacial PV modelling, Sol. Energy 218 (2021) 587–595, https://doi.org/10.1016/j.solener.2021.03.006.

[8] R. Kopecek, J. Libal, Bifacial photovoltaics 2021: status, opportunities and challenges, Energies 14 (2021), https://doi.org/10.3390/en14082076.

[9] X. Sun, M.R. Khan, C. Deline, M.A. Alam, Optimization and performance of bifacial solar modules: a global perspective, Appl. Energy 212 (2018) 1601–1610, https://doi.org/10.1016/J.APENERGY.2017.12.041.

[10] W. Muehleisen, J. Loeschnig, M. Feichtner, A.R. Burgers, E.E. Bende, S. Zamini, Y. Yerasimou, J. Kosel, C. Hirschl, G.E. Georghiou, Energy yield measurement of an elevated PV system on a white flat roof and a performance comparison of monofacial and bifacial modules, Renew. Energy 170 (2021) 613–619, https://doi.org/10.1016/j.renene.2021.02.015.

[11] M.W.P.E. Lamers, E. Özkalay, R.S.R. Gali, G.J.M. Janssen, A.W. Weeber, I.G. Romijn, B.B. van Aken, Temperature effects of bifacial modules: hotter or cooler? Sol. Energy Mater. Sol. Cell. 185 (2018) 192–197, https://doi.org/10.1016/j.solmat.2018.05.033.

[12] N. Riedel-Lyngskær, M. Ribaconka, M. Pó, A. Thorseth, S. Thorsteinsson, C. Dam-Hansen, M.L. Jakobsen, The effect of spectral albedo in bifacial photovoltaic performance, Sol. Energy 231 (2022) 921–935, https://doi.org/10.1016/j.solener.2021.12.023.

[13] E. Mouhib, L. Micheli, F.M. Almonacid, E.F. Fernández, Overview of the fundamentals and applications of bifacial photovoltaic technology: agrivoltaics and aquavoltaics, Energies 15 (2022), https://doi.org/10.3390/en15238777.

[14] T. Baumann, H. Nussbaumer, M. Klenk, A. Dreisiebner, F. Carigiet, F. Baumgartner, Photovoltaic systems with vertically mounted bifacial PV modules in combination with green roofs, Sol. Energy 190 (2019) 139–146, https://doi.org/10.1016/j.solener.2019.08.014.

[15] A. al Mehadi, M.A. Chowdhury, M.M. Nishat, F. Faisal, M.M. Islam, A software-based approach in designing a rooftop bifacial PV system for the North Hall of Residence, IUT, Clean Energy 5 (2021) 403–422, https://doi.org/10.1093/ce/zkab019.

[16] S.-H. Yoo, H.-J. Choi, Solar architecture integrated Bi-facial photovoltaic system as a shade, Processes 9 (2021) 1625, https://doi.org/10.3390/pr9091625.

[17] M. Chen, W. Zhang, L. Xie, B. He, W. Wang, J. Li, Z. Li, Improvement of the electricity performance of bifacial PV module applied on the building envelope, Energy Build. 238 (2021), 110849, https://doi.org/10.1016/j.enbuild.2021.110849.

[18] S. Boixo, M. Diaz-Vicente, A. Colmenar, M.A. Castro, Potential energy savings from cool roofs in Spain and Andalusia, Energy 38 (2012) 425–438, https://doi.org/10.1016/j.energy.2011.11.009.

[19] J. Testa, M. Krarti, A review of benefits and limitations of static and switchable cool roof systems, Renew. Sustain. Energy Rev. 77 (2017) 451–460, https://doi.org/10.1016/j.rser.2017.04.030.

[20] H. Akbari, R. Levinson, L. Rainer, Monitoring the energy-use effects of cool roofs on California commercial buildings, Energy Build. 37 (2005) 1007–1016, https://doi.org/10.1016/j.enbuild.2004.11.013.

[21] C. Romeo, M. Zinzi, Impact of a cool roof application on the energy and comfort performance in an existing non-residential building. A Sicilian case study, Energy Build. 67 (2013) 647–657, https://doi.org/10.1016/j.enbuild.2011.07.023.

[22] M.C. Yew, M.K. Yew, L.H. Saw, T.C. Ng, K.P. Chen, D. Rajkumar, J.H. Beh, Experimental analysis on the active and passive cool roof systems for industrial buildings in Malaysia, J. Build. Eng. 19 (2018) 134–141, https://doi.org/10.1016/j.jobe.2018.05.001.

[23] A. Dominguez-Delgado, H. Domínguez-Torres, C.-A. Domínguez-Torres, Energy and economic Life cycle assessment of cool roofs applied to the refurbishment of social housing in southern Spain, Sustainability 12 (2020) 5602, https://doi.org/10.3390/su12145602.

[24] M. Hu, B. Zhao, Suhendri, J. Cao, Q. Wang, S. Riffat, Y. Su, G. Pei, Quantitative characterization of the effect of inclination angle on flat-plate radiative cooling performance in buildings, J. Build. Eng. 59 (2022), https://doi.org/10.1016/j.jobe.2022.105124.

[25] A.H.A. Dehwah, M. Krarti, Energy performance of integrated adaptive envelope technologies for commercial buildings, J. Build. Eng. 63 (2023), https://doi.org/10.1016/j.jobe.2022.105535.
[26] S.E. Bretz, H. Akbari, Long-term performance of high-albedo roof coatings, Energy Build. 25 (1997) 159–167, https://doi.org/10.1016/S0378-7788(96)01005-5.
[27] J.S. Stein, D. Riley, M. Lave, C. Hansen, C. Deline, F. Toor, Outdoor field performance from bifacial photovoltaic modules and systems, in: 2017 IEEE 44th Photovoltaic Specialist Conference (PVSC), IEEE, 2017, pp. 3184–3189, https://doi.org/10.1109/PVSC.2017.8366042.
[28] J.S. Stein, L. Burnham, M. Lave, One Year Performance Results for the Prism Solar Installation at the New Mexico Regional Test Center: Field Data from February 15, 2016 - February 14, 2017, 2017. Albuquerque.
[29] C. Ghenai, F.F. Ahmad, O. Rejeb, M. Bettayeb, Artificial neural networks for power output forecasting from bifacial solar PV system with enhanced building roof surface Albedo, J. Build. Eng. 56 (2022), https://doi.org/10.1016/j.jobe.2022.104799.
[30] H. Al-Sallal, M. Hamdan, Bifacial photovoltaic (PV) systems performance enhancement using a selective surface reflector, International Journal on Energy Conversion 10 (2022) 37–44, https://doi.org/10.15866/irecon.v10i2.21609.
[31] G.B. Cavadini, L.M. Cook, Green and cool roof choices integrated into rooftop solar energy modelling, Appl. Energy 296 (2021), 117082, https://doi.org/10.1016/j.apenergy.2021.117082.
[32] Abolin Co, Cool Barrier Technology and Photovoltaic Roof Systems Applications Guide, 2012.
[33] Soprasolar - Soprema, Combining Cool Roof & Bifacial, (n.d.). https://www.soprasolar.com/en/reflexe-solaire (accessed December 22, 2022)..
[34] Opsun, Bifacial PV : A New Approach to Rooftop PV Design, (n.d.). https://opsun.com/en/info/bifacial-pv-a-new-approach-to-rooftop-pv-design/(accessed December 22, 2022)..
[35] H. Lim, S.H. Cho, J. Moon, D.Y. Jun, S.H. Kim, Effects of reflectance of backsheets and spacing between cells on photovoltaic modules, Appl. Sci. 12 (2022) 443, https://doi.org/10.3390/app12010443.
[36] A. Sinha, D.B. Sulas-Kern, M. Owen-Bellini, L. Spinella, S. Ulĭcńa, S.A. Pelaez, S. Johnston, L.T. Schelhas, Glass/glass photovoltaic module reliability and degradation: a review, J. Phys. D Appl. Phys. 54 (2021), https://doi.org/10.1088/1361-6463/ac1462.
[37] S. Bouchakour, D. Valencia-Caballero, A. Luna, E. Roman, E.A.K. Boudjelthia, P. Rodríguez, Modelling and simulation of bifacial pv production using monofacial electrical models†, Energies 14 (2021) https://doi.org/10.3390/en14144224.
[38] IEC TC 82, IEC 61724-1 Photovoltaic system performance, Part 1 (2021). Monitoring.
[39] M. Leonardi, R. Corso, R.G. Milazzo, C. Connelli, M. Foti, C. Gerardi, F. Bizzarri, S.M.S. Privitera, S.A. Lombardo, The effects of module temperature on the energy yield of bifacial photovoltaics: data and model, Energies 15 (2022), https://doi.org/10.3390/en15010022.